Small quadrupole deformation for the dipole bands in ^{112}In

T. Trivedi,[1] R. Palit,[1,*] J. Sethi,[1] S. Saha,[1] S. Kumar,[2] Z. Naik,[1] V. V. Parkar,[1,†] B. S. Naidu,[1] A. Y. Deo,[1] A. Raghav,[1] P. K. Joshi,[1] H. C. Jain,[1] S. Sihotra,[3] D. Mehta,[3] A. K. Jain,[4] D. Choudhury,[4] D. Negi,[5] S. Roy,[6] S. Chattopadhyay,[6] A. K. Singh,[7] P. Singh,[7] D. C. Biswas,[8] R. K. Bhowmik,[5] S. Muralithar,[5] R. P. Singh,[5] R. Kumar,[5] and K. Rani[5]

[1]*Department of Nuclear and Atomic Physics, Tata Institute of Fundamental Research, Mumbai 400005, India*

[2]*Department of Physics and Astrophysics, University of Delhi, Delhi 110007, India*

[3]*Department of Physics, Panjab University, Chandigarh 160014, India*

[4]*Department of Physics, Indian Institute of Technology, Roorkee 247667, India*

[5]*Inter University Accelerator Centre, New Delhi 110067, India*

[6]*Saha Institute of Nuclear Physics, I/AF, Bidhannagar, Kolkata 700064, India*

[7]*Department of Physics & Meteorology, Indian Institute of Technology Kharagpur, Kharagpur 721302, India*

[8]*Nuclear Physics Division, Bhabha Atomic Research Centre, Mumbai 400085, India*

(Received 27 October 2011; published 26 January 2012)

High spin states in ^{112}In were investigated using the ^{100}Mo(^{16}O, $p3n$) reaction at 80 MeV. The excited level has been observed up to 5.6 MeV excitation energy and spin $\sim 20\hbar$ with the level scheme showing three dipole bands. Polarization and lifetime measurements were carried out for the dipole bands. Tilted axis cranking model calculations were performed for different quasiparticle configurations of this doubly odd nucleus. Comparison of the calculations of the model with the $B(M1)$ transition strengths of the positive- and negative-parity bands firmly established their configurations.

DOI: 10.1103/PhysRevC.85.014327 PACS number(s): 21.10.Hw, 21.60.Jz, 25.70.Gh, 27.60.+j

I. INTRODUCTION

Various nuclear excitation modes have been understood by considering the symmetry of the nuclear mean field and the relative orientation of the total angular momentum with respect to its principal axes. In particular, the investigation of generating high angular momentum states in nuclei based on symmetry considerations and geometrical models has been extremely successful in novel excitation modes such as magnetic, antimagnetic, and chiral rotations [1]. Studies of high spin states in Ag, Cd, and In near $A \sim 110$ isotopes continue to reveal new aspects of these modes of excitations in nuclei [2–6]. Magnetic rotational (MR) bands were reported in ^{108,110}In isotopes [7] and, recently, two dipole bands observed in ^{106}In were explained in terms of different K values with the same quasiparticle orbitals [8,9]. The nuclei in this region exhibit many exciting features involving regular band structures arising from the occupancy of the valance protons and neutrons in $g_{9/2}$ and $h_{11/2}$ orbitals, respectively. Such high-j orbitals are now well known for generation of rotation-like sequences of $M1$ transitions called shears bands [10]. Another interesting aspect of nuclei in this mass region is the appearance of nearly degenerate $\Delta I = 1$ doublet bands [11–13] with the same parity. In this picture, the degenerate bands observed in the laboratory frame arise in nuclei due to the possibility of forming mutually perpendicular coupling of three angular momenta of the collective triaxial core, valence neutron, and proton either in a left- or right-handed system in the intrinsic frame of the nucleus. Relativistic mean-field (RMF) calculations have been reported for the odd-odd nuclides in the $A \sim 100$ mass region [14]. Favorable γ deformation required for chirality has been predicted in $^{102–110}$Rh, $^{108–112}$Ag, and ^{112}In odd-odd isotopes. These triaxial doubly odd isotopes are predicted to have multiple chiral bands. Recently, ^{112}In has attracted considerable experimental attention and an elaborate level scheme of ^{112}In has been reported in Ref. [15] based on the ^{7}Li + ^{110}Pd reaction. One of the motivations of the present work is to assign the parity of different dipole bands through polarization measurements for detailed understanding of their configurations. In addition, a heavier ion beam was chosen to populate excited levels of ^{112}In with higher recoil velocity required for lifetime measurements using the Doppler-shift attenuation method (DSAM). The results of polarization and lifetime measurements have been used along with tilted axis cranking (TAC) calculations [17,18] to obtain the shape parameters and quasiparticle configurations for different bands in ^{112}In. The present experimental details and results are discussed in Secs. II and III.

II. EXPERIMENTAL DETAILS AND ANALYSIS PROCEDURE

High spin states in ^{112}In were populated using the ^{100}Mo(^{16}O, $p3n$) reaction. The 80-MeV ^{16}O beam was obtained from the 15-UD Pelletron accelerator at IUAC, New Delhi. The target consisted of 2.7 mg/cm^2 ^{100}Mo with a backing of $\sim$12 mg/cm^2 Pb to stop the recoiling ions produced in the reaction. The Indian National Gamma Array (INGA) consisting of eighteen Compton-suppressed clover detectors was used to detect γ rays emitted in the reaction. This collaborative research facility was initiated by Tata Institute of Fundamental Research, IUAC, Bhabha Atomic Research Centre,

*palit@tifr.res.in

†Present address: Departamento de Física Aplicada, Universidad de Huelva, E-21071 Huelva, Spain.

Saha Institute of Nuclear Physics, Variable Energy Cyclotron Centre, UGC-DAE-Consortium for Scientific Research, and many universities in India. The clover detectors were arranged in five rings, at 32°, 57°, 90°, 123°, and 148° with respect to the beam direction [19,20]. The data were acquired when at least three clover detectors fired simultaneously. ^{133}Ba and ^{152}Eu radioactive sources were used for the energy calibration and determination of relative photopeak efficiency of the array. After gain matching of individual crystals, add-back spectra were generated for all the clovers and the coincidence data were stored in the γ-γ matrix, which has about 1.1×10^9 events in total. An $E_\gamma \times E_\gamma \times E_\gamma$ cube was also constructed from the data. The RADWARE software package [21] was used for the analysis of these matrices and the cube. The partial level scheme of ^{112}In is shown in Fig. 1. Various gated spectra relevant for identifying transitions in bands A, B, and C are shown in Figs. 2–4. The double-gated spectrum obtained in coincidence with 319- and 261-keV transitions shown in Fig. 2 depicts the 128–178–273–393–554–708-keV cascade of band A. Similarly, the four double-gated spectra given in Figs. 3 and 4 with gates on 187–297-, 187–437-, 588–297-, and 588–437-keV transition pairs show the γ rays of bands B and C as given in Refs. [15,16].

The directional correlation of oriented states (DCO) and integrated polarization direction correlation (IPDCO) analysis were carried out to determine the spin and parity of different states (see Table I). The multipolarity of γ rays were deduced from the angular correlation analysis [22] using the method of directional correlation from oriented states ratios of two coincident γ rays, γ_1 and γ_2, given by

$$R_{DCO} = \frac{I\gamma_1 \text{ observed at } 32^\circ \text{ gated on } \gamma_2 \text{ at } 90^\circ}{I\gamma_1 \text{ observed at } 90^\circ \text{ gated on } \gamma_2 \text{ at } 32^\circ}.$$

In the present geometry of detectors, the DCO ratios obtained with a stretched quadrupole (dipole) gate are 0.5(1.0) and 1.0(2.0) for the pure dipole and quadrupole transitions, respectively. The DCO ratios obtained are shown in Fig. 5. The extracted DCO values were obtained with a gate on the strong $\Delta I = 1$ dipole transitions.

The clover detectors at 90° were used as a Compton polarimeter, which helps in identifying the electric or magnetic

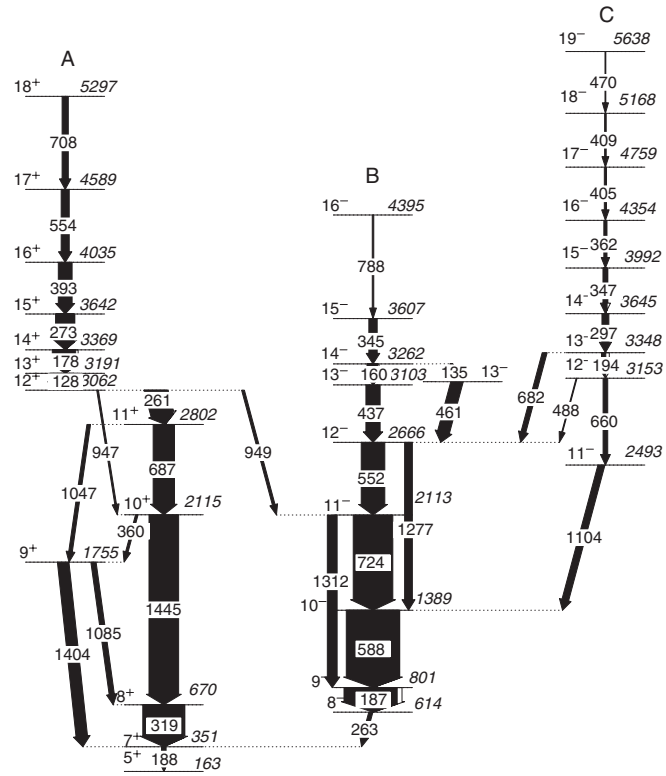

FIG. 1. Partial level scheme of ^{112}In relevant for the present work. The γ-ray energies are in keV.

nature of the γ rays [23,24]. For a Compton polarimeter, the polarization asymmetry Δ of the transition is defined as [23]

$$\Delta = \frac{a(E_\gamma)N_\perp - N_\parallel}{a(E_\gamma)N_\perp + N_\parallel}, \quad (1)$$

where $N_\perp$ ($N_\parallel$) is the number of counts of γ transitions scattered perpendicular (parallel) to the reaction plane. The correction factor $a(E_\gamma)$ is a measure of the perpendicular to parallel scattering asymmetry within the crystals of the clover. For the 90° detectors this parameter has been found to be 0.98(1) from the analysis of decay data of the ^{152}Eu radioactive source. For linear polarization measurement, two

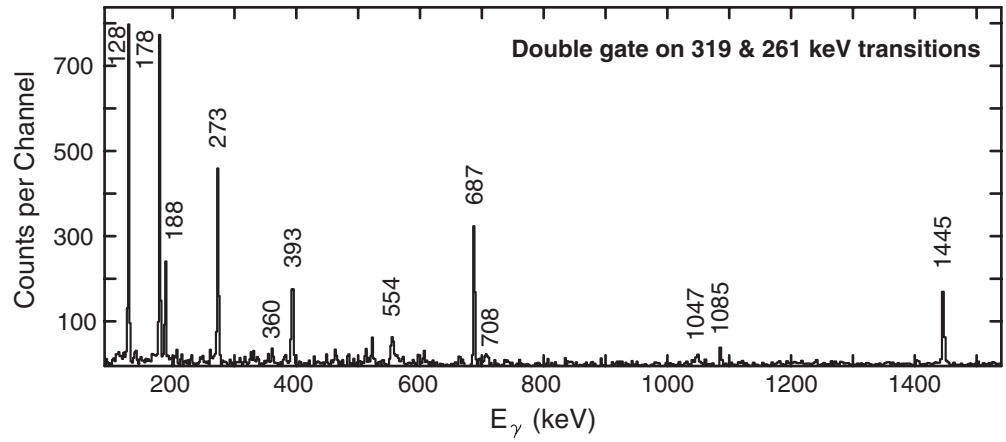

FIG. 2. Double-gated spectrum with 319- and 261-keV transitions indicating all the dipole transitions of band A.

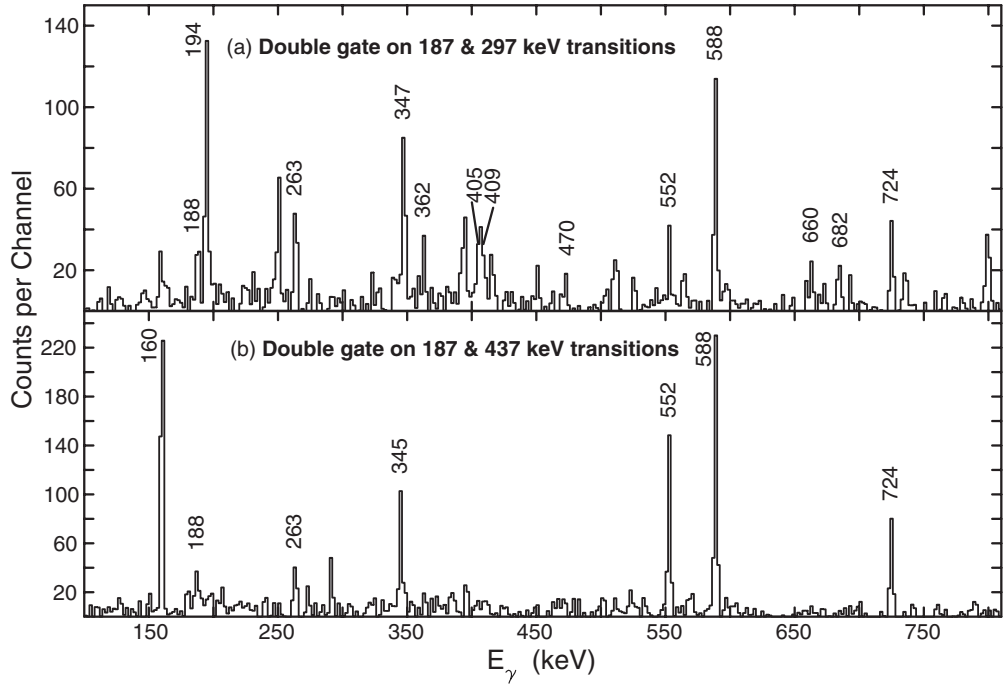

FIG. 3. Double-gated spectra obtained by (a) gates on 187- and 297-keV transitions and (b) 187- and 437-keV transitions. γ-ray transitions associated with ^{112}In, labeled with their energies in keV.

asymmetric matrices corresponding to parallel and perpendicular segments of the clover detectors (with respect to the emission plane) along one axis and the coincident γ rays along the other axis were constructed [25]. Then an IPDCO analysis was carried out. A positive value of the IPDCO ratio indicates an electric transition while a negative value indicates a magnetic transition. The positive and negative asymmetry parameters of different transitions depicted in Fig. 6 indicate their electric and magnetic nature, respectively. The 261-keV-gated spectra generated from parallel ($N_\parallel$) and perpendicular [$a(E_\gamma)N_\perp$] scattering events observed in the 90° clover detectors are shown in Fig. 7. The higher counts of the

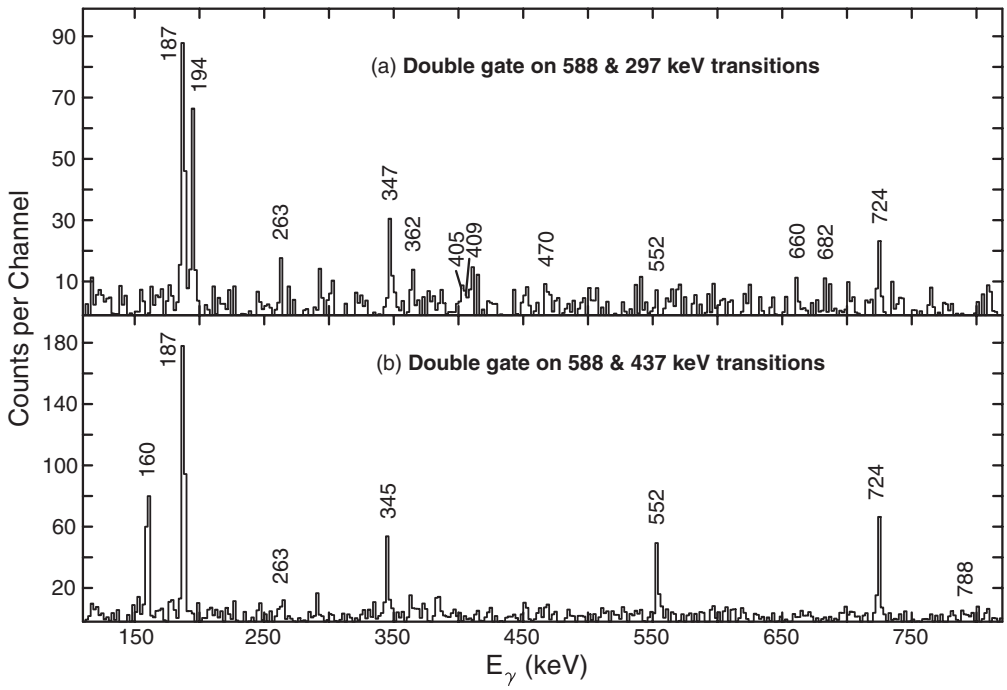

FIG. 4. Double-gated spectra obtained by (a) gates on 588- and 297-keV transitions and (b) 588- and 437-keV transitions. γ-ray transitions associated with ^{112}In are labeled with their energies in keV.

TABLE I. Excitation energies, γ-ray energies, intensities, DCO ratios, multipolarities, IPDCO values, and initial- and final-state spins of the transitions of ^{112}In deduced from the present work. The uncertainties in the energies of γ rays are 0.3 keV for intense peaks and 0.7 keV for weak peaks.

E_x (keV)	E_γ (keV)	I_γ	$R_{DCO}(D)$	Multipolarity	IPDCO	$I_i^\pi \rightarrow I_f^\pi$
614	263.1		1.17(10)			$8^- \rightarrow 7^+$
670	319.2	104.3(8)	1.06(7)	$M1$	−0.079(28)	$8^+ \rightarrow 7^+$
801	187.1					$9^- \rightarrow 8^-$
1389	588.2	134.8(9)	0.96(7)	$M1$	−0.037(23)	$10^- \rightarrow 9^-$
1755	1084.8	13.1(1)	1.22(10)	$M1$	−0.095(59)	$9^+ \rightarrow 8^+$
	1404.0	29.1(13)	1.96(15)	$E2$	0.079(33)	$9^+ \rightarrow 7^+$
2113	724.3	100(6)	1.02(6)	$M1$	−0.057(25)	$11^- \rightarrow 10^-$
	1312.5	24.8(4)	1.69(14)	$E2$	0.235(42)	$11^- \rightarrow 9^-$
2115	1445.2	75.1(4)	1.69(12)	$E2$	0.058(27)	$10^+ \rightarrow 8^+$
	360.4	6.1(1)	1.21(11)			$10^+ \rightarrow 9^+$
2493	1104.2	17.2(2)	1.16(9)	$M1$	−0.015(48)	$11^- \rightarrow 10^-$
2666	552.4	59.4(4)	1.02(6)	$M1$	−0.099(42)	$12^- \rightarrow 11^-$
	1276.7	19.6(2)	1.85(18)	$E2$	0.157(73)	$12^- \rightarrow 10^-$
2802	686.9	53.9(3)	1.03(7)	$M1$	−0.078(27)	$11^+ \rightarrow 10^+$
	1047.4	9.1(1)	1.78(13)	$E2$	0.116(42)	$11^+ \rightarrow 9^+$
3062	260.6	56.9(2)	0.97(7)	$M1$	−0.030(38)	$12^+ \rightarrow 11^+$
	947.4	4.2(2)				$12^+ \rightarrow 10^+$
	949.1	6.8(3)				$12^+ \rightarrow 11^-$
3103	437.1	35.6(3)	0.98(6)	$M1$	−0.013(43)	$13^- \rightarrow 12^-$
3127	461.4	30.3(2)	0.80(5)	$M1$	−0.127(30)	$13^- \rightarrow 12^-$
3153	660.2	11.7(3)	0.94(9)	$M1$	−0.047(46)	$12^- \rightarrow 11^-$
	487.7	2.2(1)				$12^- \rightarrow 12^-$
3191	128.3	60.1(2)	1.21(13)			$13^+ \rightarrow 12^+$
3262	159.6	26.7(2)	0.97(9)			$14^- \rightarrow 13^-$
	135.3	6.1(1)	1.09(11)			$14^- \rightarrow 13^-$
3348	194.2	10.8(1)	0.99(9)			$13^- \rightarrow 12^-$
	681.9	12.1(2)	0.95(6)			$13^- \rightarrow 12^-$
3369	178.5	59.3(2)	1.06(9)			$14^+ \rightarrow 13^+$
3607	344.6	20.7(1)	1.01(9)			$15^- \rightarrow 14^-$
3642	272.7	47.2(2)	0.91(6)	$M1$	−0.090(39)	$15^+ \rightarrow 14^+$
3645	296.9	17.0(2)	0.86(7)	$M1$	−0.039(40)	$14^- \rightarrow 13^-$
3992	347.1	10.4(1)	1.01(9)			$15^- \rightarrow 14^-$
4035	393.3	34.5(2)	1.10(7)	$M1$	−0.139(26)	$16^+ \rightarrow 15^+$
4354	362.4	7.8(1)	0.91(7)			$16^- \rightarrow 15^-$
4395	787.9	3.8(1)	0.89(7)			$16^- \rightarrow 15^-$
4589	554.2	20.3(2)	0.89(6)	$M1$	−0.157(44)	$16^+ \rightarrow 15^+$
4759	404.7	5.4(1)	0.74(7)			$17^- \rightarrow 16^-$
5168	409.2	3.9(1)	1.00(9)			$18^- \rightarrow 17^-$
5297	707.6	15.6(1)				$18^+ \rightarrow 17^+$
5638	470.0	2.0(1)	0.92(7)			$19^- \rightarrow 18^-$

273-, 319-, and 393-keV transitions in the parallel scattering spectrum compared to those in perpendicular scattering spectra suggested their magnetic nature, while the reverse nature of the spectra for the 1445-keV transition confirms its electric multipolarity.

For the application of the DSAM, line shapes were obtained from the background-subtracted spectra projected from the two matrices consisting of events in the 148° or 32° detectors along one axis and all other detectors along the second axis, respectively. These matrices contained approximately 5.8×10^8 and 4.0×10^8 coincidence events, respectively. The forward and backward Doppler-shifted line shapes of 273-, 393-, and 554-keV transitions are shown in Fig. 8. The line-shape spectra were generated by putting a gate on the transition below the level of interest.

III. ANALYSIS RESULTS

A. DCO and polarization measurements

The DCO values of the transitions from the higher levels are obtained with a gate on the 319-keV transition. The polarization asymmetry values of the 319-, 1445-, and 687-keV transitions confirm the positive parity for the 11^+ level at an excitation energy of 2802 keV. The 128–178–273–393–554–708-keV cascade present in the 319- and 261-keV

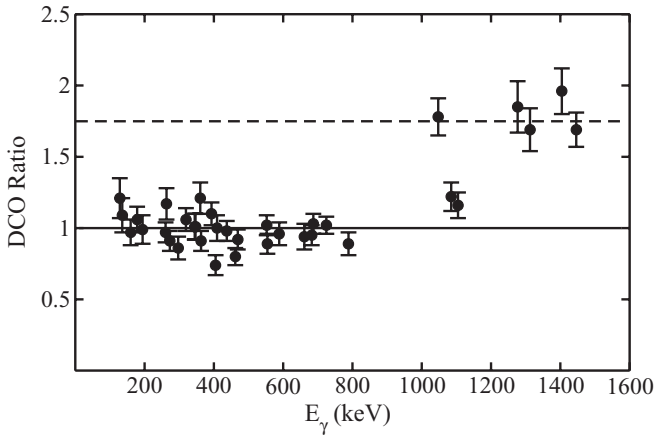

FIG. 5. Plot for DCO ratios of different transitions.

double-gated spectrum shown in Fig. 2 feeds the 2802-keV level through the 261-keV transition. Polarization and DCO values obtained for the 261-keV transition establishes the positive parity of band A. The polarization asymmetries for 273-, 393-, and 554-keV transitions are found to be negative, suggesting their magnetic character. The IPDCO of low-energy 128- and 178-keV transitions could not be extracted and are assumed to be magnetic based on the systematics of the dipole bands in this mass region. Further, an $E2/M1$ multipole mixing ratio analysis [22] was carried out for the dipole transitions of band A (273, 393, and 554 keV), from their extracted R_{DCO} values with a gate on the 319-keV pure $\Delta I = 1$ transition. The measured R_{DCO} ratios suggest that these γ rays have a small $E2/M1$ multipole mixing ratio at $-7^\circ < \arctan(\delta) < -1^\circ$. This along with the IPDCO measurements suggests a pure $M1$ nature for these intraband $\Delta I = 1$ transitions.

The transitions of bands B and C were obtained from the double-gated spectra given in Figs. 3 and 4. The double-gated spectra obtained with 187–437-keV and 588–437-keV pair of transitions suggest placement of the 160–345–788-keV cascade above the 3103-keV state with $I^\pi = 13^-$. The transitions placed in band C are shown in Figs. 3 and 4 in the spectra obtained with 187–97- and 588–297-keV pairs. The bandhead of band C was assigned a negative parity with spin

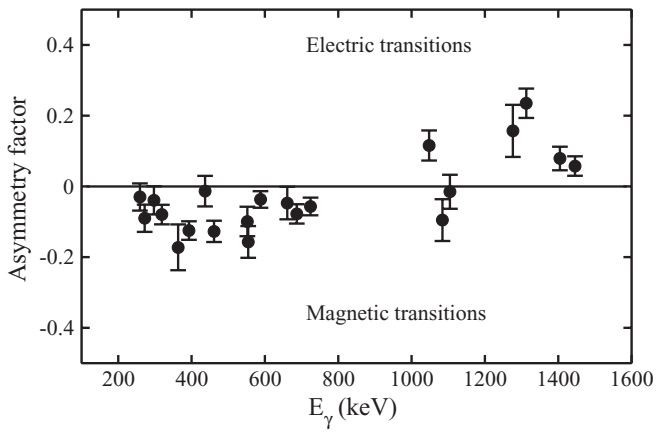

FIG. 6. Plot for polarization asymmetry for different transitions.

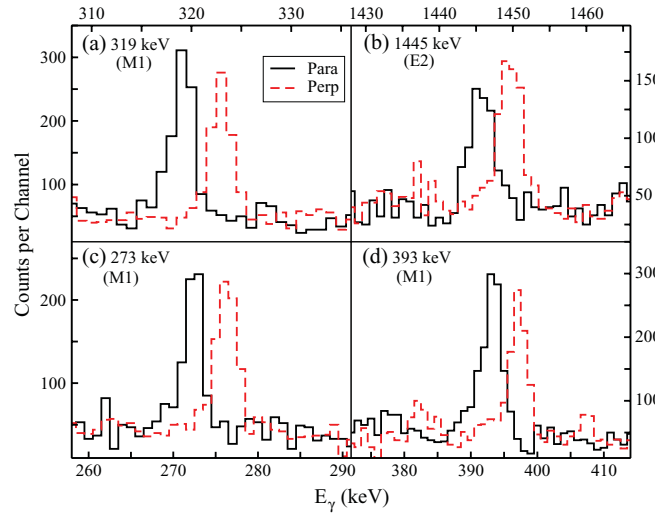

FIG. 7. (Color online) 261-keV gated spectra of the perpendicular and parallel Compton scattering in the 90° clover detectors corresponding to (a) 319-keV, (b) 1445-keV, (c) 273-keV, and (d) 393-keV transitions. Higher counts for 273-, 319-, and 393-keV transitions in the parallel scattered spectrum indicates their magnetic character, while (b) suggests an electric nature for the 1445-keV transition. An offset of 4 keV has been introduced between the parallel and perpendicular spectra for clarity.

11^- due to the measured DCO and IPDCO of the 1104- and 660-keV transitions. Two more interband transitions between bands B and C with energy of 488 and 682 keV are also observed in the gated spectrum. The 194–297–347–362–405–409–470-keV cascade was reported in Ref. [16]. This band C has a lower yield in the present reaction compared to band A. Therefore, only the IPDCO of the 297-keV transition could be extracted and found to have a magnetic nature. The DCO ratios for the 194-, 297-, 347-, and 362-keV transitions are found to be around 1.0, suggesting $\Delta I = 1$ for these transitions.

B. Lifetime measurements

Lifetimes of the states of bands A and C have been measured by DSAM. In the analysis, gating transitions were below the transitions of interest. For analyzing the line shapes of different transitions of ^{112}In, the LINESHAPE [26] program was used. The program takes into account the energy loss of the beam through the target and the energy loss and angular straggling of the recoils through the target and the backing. For the energy-loss calculations, we have used the shell-corrected Northcliffe and Schilling stopping powers [27]. The value of the time step and the number of recoil histories were chosen to be 0.01 ps and 5000, respectively. In the fitting procedure, the program obtains a χ^2 minimization of the fit for transition quadrupole moments (Q_t) for the transition of interest, transition quadrupole moments Q_t(SF) of the modeled side-feeding cascade, the intensity of contaminant peaks in the region of interest, and the normalizing factor to normalize the intensity of the fitted transition. The best fit was

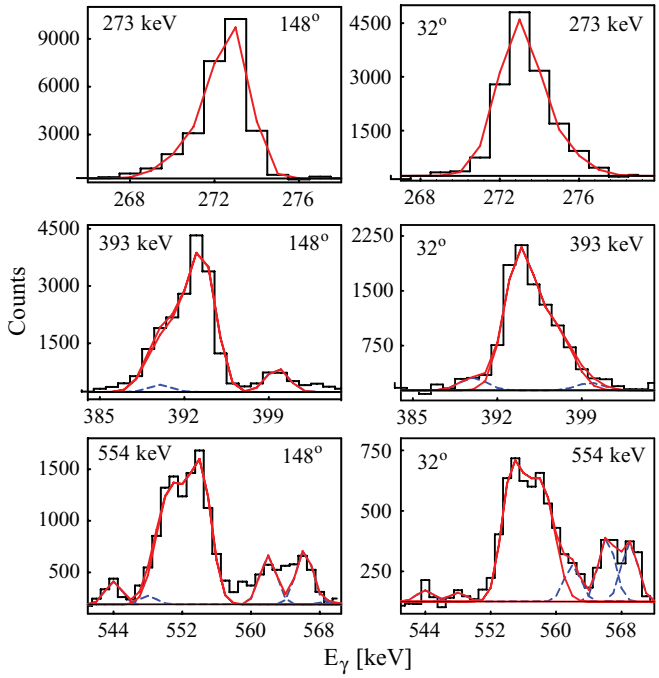

FIG. 8. (Color online) Representative spectra (with gate on the lower transition) along with theoretically fitted line shapes for 273-, 393-, and 554-keV transitions in the positive-parity yrast band of ^{112}In for γ-ray spectra at 32°, and 148° with respect to the beam direction. The contaminant peaks are marked by dashed lines.

obtained through the least-square-minimization procedures SEEK, SIMPLEX, and MIGRAD referred to in Ref. [26]

In band A, the Doppler-broadened line shapes were observed for the 273-, 393-, 554-, and 708-keV transitions above the $I^\pi = 14^+$ state. The line shapes of these transition were obtained by putting gate on the 178-keV transition. By assuming 100% side feeding into the top of band, an effective lifetime of the top-most state was estimated; this was then used as an input parameter to extract the lifetimes of lower states in the cascade. The side feeding into each level of the band was considered as a cascade of five transitions having a fixed moment of inertia comparable to that of the in-band sequences. The energies of γ rays and side-feeding intensities were used as input parameters for the line-shape analysis. Side-feeding intensities were calculated by using an asymmetric γ-γ matrix comprising γ rays detected by detectors at 90° along one axis and all other detectors along the second axis. Once the χ^2 minimization was obtained by the MINUIT [28] program, the background and the contaminant peak parameters were fixed and the procedure was followed for the next lower level. After obtaining a χ^2 minimization for each level, a global fit was carried out, with the background and the contaminant peak parameters of all the levels kept fixed. The side-feeding lifetimes were found to be faster than the level lifetimes, similar to the measurements reported in nearby nuclei in this mass region [7,17].

The final lifetime values were obtained by taking weighted averages of the results obtained from the two separate fits which were performed at 32° and 148°. For each band, $B(M1)$ values were calculated from measured lifetimes using the following relationship:

$$B(M1) = \frac{0.05697}{E_\gamma^3(M1)\tau\,[1+\alpha_t(M1)]}\,[\mu_N^2], \qquad (2)$$

where E_γ is the transition energy in MeV, τ is the partial lifetime of the transition deduced from the fitted line shape of the state, and α_t is total internal conversion coefficient of the transition, respectively. These results are listed in Table II and fitting of the theoretical line shapes with the experimental data for 273-, 393-, and 554-keV transitions are shown in Fig. 8. The errors quoted in lifetimes do not include the systematic errors from the uncertainty in stopping power, which can be as large as 15%. Similarly, line shapes for 347- and 362-keV transitions of band C were observed. After the fitting of calculated line shapes, the lifetime of the respective states are given in Table II.

TABLE II. Lifetimes of the states and reduced $B(M1)$ strengths of transitions of ^{112}In.

I_i^π	$E_{\gamma,M1}$ (keV)	τ (ps)	$B(M1)$ $(\mu_N)^2$
15^+	272.7	$0.83^{+0.04}_{-0.04}$	$3.28^{+0.14}_{-0.14}$
16^+	393.3	$0.49^{+0.03}_{-0.03}$	$1.89^{+0.11}_{-0.10}$
17^+	554.2	$0.22^{+0.02}_{-0.03}$	$1.52^{+0.20}_{-0.14}$
18^+	707.6	<0.25	>0.63
15^-	347.1	$0.72^{+0.25}_{-0.16}$	$1.87^{+0.55}_{-0.48}$
16^-	362.4	<0.60	>1.97

IV. COMPARISON WITH MODEL CALCULATIONS

The positive-parity dipole band with bandhead excitation energy of 3.062 MeV has been observed up to $I^\pi = 18^+$. Similar dipole bands have been observed in ^{108}In and ^{110}In with a $\pi g_{9/2}^{-1} \otimes \nu(d_{5/2}/g_{7/2})(h_{11/2})^2$ quasiparticle configuration [7]. Figure 9 demonstrates the comparison of experimentally determined $B(M1)$ transition strengths as a function of the spin for the dipole band of ^{112}In with band 3 of ^{108}In and ^{110}In [7] having almost similar configurations. It is evident that the $B(M1)$ strength decreases with increasing spin up to $I^\pi = 18^+$ in an identical way for all three dipole bands, which confirms the similar configuration for the positive-parity dipole band of ^{112}In. In addition, it is to be noted that the band crossing near $\hbar\omega = 0.6$ MeV observed in these positive-parity dipole bands of ^{108,110}In is not seen in ^{112}In [7,15]. Very recently, a positive-parity dipole band with a bandhead spin of $I^\pi = 11^+$ has been assigned the same configuration $\pi g_{9/2}^{-1} \otimes \nu(d_{5/2}/g_{7/2})(h_{11/2})^2$ in ^{114}In [29]. This band has strong $\Delta I = 1$ transitions with unobserved crossover $E2$ transitions and no signature splitting, similar to the lighter odd-odd In isotopes. It will be interesting to perform lifetime measurements for the levels in this band of ^{114}In to confirm the role of the shear mechanism.

In the discussion that follows, the experimental data of the dipole bands (labeled as A and C) are compared with the results of TAC model calculations. Values for the proton pairing gap parameter of $\Delta_\pi = 0.99$ MeV and for the neutron pairing gap parameter of $\Delta_\nu = 0.85$ MeV were used in the TAC calculations. These values are 0.6 and 0.8 times the

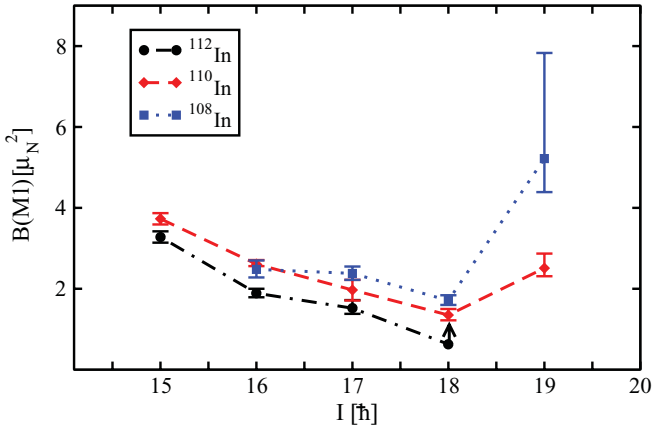

FIG. 9. (Color online) Comparison of experimentally measured $B(M1)$ transition strength as a function of spin for dipole band 3 of ^{108}In, ^{110}In [7], and band A of ^{112}In.

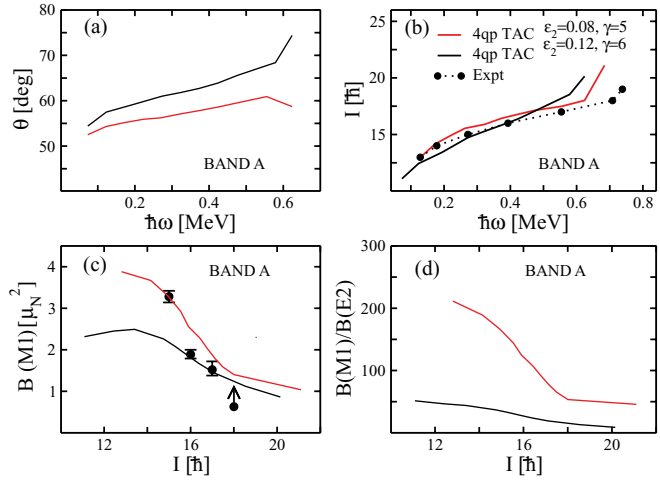

FIG. 10. (Color online) The results of TAC calculations for the positive-parity band showing (a) the variation of tilt angle with rotational frequency, (b) spin (I) vs rotational frequency, (c) $B(M1)$ transition strength vs spin, and (d) $B(M1)/B(E2)$ ratio vs spin. The experimental data shown as filled circles for band A of ^{112}In are plotted in (b) and (c) for comparison.

odd and even mass difference, respectively. The chemical potentials λ_ν (both proton and neutron) were chosen so that a particle number is conserved for $Z = 49$ and $N = 63$. The values of the deformation parameters ϵ_2 and γ were obtained by Nilsson Strutinsky's minimization procedure [30]. The nature of band A, which is a $\Delta I = 1$ positive-parity $M1$ band, was investigated. A quasiparticle configuration $\pi g_{9/2}^{-1} \otimes \nu(d_{5/2}/g_{7/2})(h_{11/2})^2$ is used in TAC calculations for the dipole band. Similar configurations have been assigned in lighter odd-odd In isotopes and supports magnetic rotations. A minimum is found at a deformation of $\epsilon_2 = 0.12$ and $\gamma = 6^\circ$. The calculated I versus $\hbar\omega$ and $B(M1)$ versus I plots based on this global minimum given in Fig. 10 qualitatively explains the measured data. However, the overall decreasing trend of the experimental $B(M1)$ values in the measured range of spin is better explained by the results of the TAC calculations based on a static deformation with $\epsilon_2 = 0.08$ and $\gamma = 5^\circ$. In particular, the measured $B(M1)$ value at lower spin ($I^\pi = 15^+$) is closer to the TAC calculation based on this lower deformation. The static minimum suggests almost a constant tilt angle of around 55° and a large $B(M1)/B(E2)$ values, which is in line with the nonobservation of crossover $E2$ transitions in band A. The low deformation of these states indicates that the contribution from the core in angular momentum generation is negligible and the whole of the angular momentum generation along the band can be attributed to the shears mechanism. Similar situations have been reported for ^{107}In [17] and ^{106,108}Sn [31] isotopes in the literature. Moreover, the good agreement between the TAC calculations with constant tilt angle and the measured variation of excitation energy and $B(M1)$ values with spin for the positive-parity band firmly establishes magnetic rotation for positive-parity band A. This positive-parity band under consideration is probably one of the ideal MR bands due to the very low deformation of 0.08. However, the confirmation of the small deformation will require further investigation of the crossover $E2$ transitions and measurement of the $B(E2)$ values. The band crossing observed at a rotational frequency of 0.6 MeV for ^{108,112}In is due to lowering of the energy of the $\pi g_{9/2}^{-1} \otimes \nu((h_{11/2})^2(g_{7/2}/d_{5/2})^3$ configuration at higher rotational frequency. Due to increasing neutron number up to $N = 63$ for ^{112}In, $g_{7/2}$ orbitals are not available near the neutron Fermi surface for this configuration to be energetically favorable, which explains the absence of band crossing for band A.

A negative-parity dipole band C studied in the present work has an excitation energy of 3153 keV. The 194–297–347–362–404–409–470-keV cascade extended band C up to $I^\pi = 19^-$. The $\pi g_{9/2}^{-1} \otimes \nu(h_{11/2})^3$ configuration has been used in TAC calculations for comparison of band C and gives a

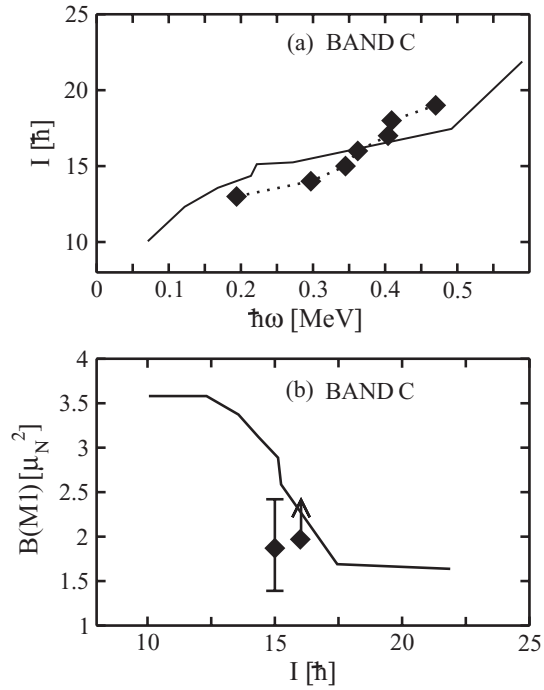

FIG. 11. The results of TAC calculations and its comparison with the experimental data for negative-parity band C of ^{112}In.

minimum with $\epsilon_2 = 0.13$ and $\gamma = 0^\circ$. The calculated I versus ω plot (Fig. 11) explains the measured values reasonably well. The measured $B(M1)$ values at $I^\pi = 15^-, 16^-$ are also reproduced with the results of TAC calculations. This confirms the quasiparticle configuration of band C. In future, it will be interesting to perform recoil distance measurements to determine the lifetime of lower states of band C for testing the prediction of higher $B(M1)$ values at lower spin states.

V. SUMMARY

In summary, polarization and lifetime measurements for the excited states of the previously established level scheme of ^{112}In have been carried out. Out of the three dipole bands observed in the present experiment, band A is found to have positive parity, while bands B and C have negative parity. The extracted $B(M1)$ values from the measured lifetime of the excited states of band A have a decreasing trend with increasing spin. The TAC calculations based on the $\pi g_{9/2}^{-1} \otimes \nu(d_{5/2}/g_{7/2})(h_{11/2})^2$ configuration reproduces the measured trend of $B(M1)$ with increasing spin. This establishes the shear rotation in ^{112}In for the positive-parity dipole band. The TAC calculations based on $\pi g_{9/2}^{-1} \otimes \nu(h_{11/2})^3$ quasiparticle configurations have been compared with the measurements for band C. The fair agreement of TAC calculations with the measurement suggests weak prolate deformation for the positive- (A) and negative-parity (C) dipole bands for ^{112}In, in contrast to the triaxial deformation as predicted in the RMF calculation [14]. Further measurement of the crossover $E2$ transitions in band A would establish this band as an ideal example of magnetic rotational band owing to its small deformation of 0.08.

ACKNOWLEDGMENTS

The authors would like to thank the IUAC Pelletron staff for providing good quality beams. The help and cooperation of the members of the INGA Collaboration for setting up the array are acknowledged. This work was partially funded by the Department of Science and Technology, Government of India (No. IR/S2/PF-03/2003-I).

[1] S. Frauendorf, Rev. Mod. Phys. **73**, 463 (2001).
[2] A. J. Simons *et al.*, Phys. Rev. Lett. **91**, 162501 (2003).
[3] S. Zhu *et al.*, Phys. Rev. C **64**, 041302(R) (2001).
[4] P. Datta *et al.*, Phys. Rev. C **71**, 041305 (2005).
[5] D. Choudhury *et al.*, Phys. Rev. C **82**, 061308(R) (2010).
[6] S. Roy *et al.*, Phys. Lett. B **694**, 322 (2011).
[7] C. J. Chiara *et al.*, Phys. Rev. C **64**, 054314 (2001).
[8] A. Y. Deo *et al.*, Phys. Rev. C **79**, 067304 (2009).
[9] R. Palit *et al.*, Nucl. Phys. A **834**, 81c (2010).
[10] R. M. Clark and A. O. Macchiavelli, Annu. Rev. Nucl. Part. Sci. **50**, 1 (2000), and references therein.
[11] C. Vaman, D. B. Fossan, T. Koike, K. Starosta, I. Y. Lee, and A. O. Macchiavelli, Phys. Rev. Lett. **92**, 032501 (2004).
[12] T. Koike, K. Starosta, and I. Hamamoto, Phys. Rev. Lett. **93**, 172502 (2004).
[13] T. Koike, Nucl. Phys. A **834**, 36c (2010).
[14] J. Meng, J. Peng, S. Q. Zhang, and S. G. Zhou, Phys. Rev. C **73**, 037303 (2006).
[15] C.Y. He *et al.*, Phys. Rev. C **83**, 024309 (2011).
[16] C. Y. He *et al.*, Nucl. Phys. A **834**, 84c (2010).
[17] D. Negi *et al.*, Phys. Rev. C **81**, 054322 (2010).
[18] S. Frauendorf, Nucl. Phys. A **557**, 259 (1993).
[19] S. Muralithar *et al.*, Nucl. Instrum. Methods Phys. Res., Sect. A **622**, 281 (2010).
[20] R. K. Bhowmik, S. Muralithar, and R. P. Singh, DAE Symp. Nucl. Phys. B **44**, 422 (2001).
[21] D. C. Radford, Nucl. Instrum. Methods Phys. Res., Sect. A **361**, 297 (1995).
[22] A. Krämer-Flecken *et al.*, Nucl. Instrum. Methods Phys. Res., Sect. A **275** 333 (1989).
[23] K. Starosta *et al.*, Nucl. Instrum. Methods Phys. Res., Sect. A **423**, 16 (1999).
[24] R. Palit *et al.*, Pramana **54**, 347 (2000).
[25] S. Lakshmi *et al.*, Nucl. Phys. A **761**, 1 (2005).
[26] J. C. Wells, ORNL Physics Division Progress, Report No. ORNL-6689, September 30, 1991.
[27] L. C. Northcliffe and R. F. Schilling, At. Data Nucl. Data Tables **7**, 233 (1970).
[28] F. James and M. Roos, Comput. Phys. Commun. **10**, 343 (1975).
[29] C. B. Li *et al.*, Eur. Phys. J. A **47**, 141 (2011).
[30] V. M. Strutinsky, Nucl. Phys. A **95**, 420 (1967).
[31] D. G. Jenkins *et al.*, Phys. Rev. Lett. **83**, 500 (1999).